An iterative method to evaluate one-dimensional pulsed nonlinear elastic wavefields and mixing of elastic waves in solids

Selvam, Sundaraelangovan; Volker, Arno; van Neer, Paul; de Jong, Nico; Verweij, Martin D.

DOI
10.1121/10.0010448

Publication date
2022

Document Version
Final published version

Published in
The Journal of the Acoustical Society of America

An iterative method to evaluate one-dimensional pulsed nonlinear elastic wavefields and mixing of elastic waves in solids

Sundaraelangovan Selvam, Arno Volker, Paul van Neer, et al.

Citation: The Journal of the Acoustical Society of America **151**, 3316 (2022); doi: 10.1121/10.0010448
View online: https://doi.org/10.1121/10.0010448
View Table of Contents: https://asa.scitation.org/toc/jas/151/5
Published by the Acoustical Society of America

JASA ARTICLE

An iterative method to evaluate one-dimensional pulsed nonlinear elastic wavefields and mixing of elastic waves in solids

Sundaraelangovan Selvam,[1,a] Arno Volker,[2] Paul van Neer,[2] Nico de Jong,[1,b] and Martin D. Verweij[1,b]
[1]*Laboratory of Medical Imaging, Department of Imaging Physics, Delft University of Technology, Delft, Netherlands*
[2]*Acoustics and Sonar, TNO, The Hague, Netherlands*

ABSTRACT:
Over the last 15 years, literature on nondestructive testing has shown that the generation of higher harmonics and nonlinear mixing of waves could be used to obtain the nonlinearity parameters of an elastic medium and thereby gather information about its state, e.g., aging and fatigue. To design ultrasound measurement setups based on these phenomena, efficient numerical modeling tools are needed. In this paper, the iterative nonlinear contrast source method for numerical modeling of nonlinear acoustic waves is extended to the one-dimensional elastic case. In particular, nonlinear mixing of two collinear bulk waves (one compressional, one shear) in a homogeneous, isotropic medium is considered, taking into account its third-order elastic constants ($\mathcal{A}$, $\mathcal{B}$, and $\mathcal{C}$). The obtained results for nonlinear propagation are in good agreement with a benchmark solution based on the modified Burgers equation. The results for the resonant waves that are caused by the one-way and two-way mixing of primary waves are in quantitative agreement with the results in the literature [Chen, Tang, Zhao, Jacobs, and Qu, J. Acoust. Soc. Am. **136**(5), 2389–2404 (2014)]. The contrast source approach allows the identification of the propagating and evanescent components of the scattered wavefield in the wavenumber-frequency domain, which provides physical insight into the mixing process and explains the propagation direction of the resonant wave.
 https://doi.org/10.1121/10.0010448
(Received 21 July 2021; revised 22 April 2022; accepted 23 April 2022; published online 20 May 2022)
[Editor: Lixi Huang]]
Pages: 3316–3327

I. INTRODUCTION

The behavior of materials under dynamic loading conditions is an important field of study in many applications such as aerospace, automotive, nondestructive testing (NDT), medical imaging, etc. In NDT methods, the classical (linear) ultrasound approaches are not sensitive enough to the microstructural damage of the materials, which is considered useful to study material integrity in the emerging field of quantitative nondestructive evaluation.[1–5] Higher harmonics generation and nonlinear wave-mixing techniques are widely applied nonlinear ultrasound approaches to evaluate the nonlinearity parameters described by three independent third-order elastic (TOE) constants, which are demonstrated to be closely related to the microstructural changes inside materials such as fatigue damages, plastic deformations,[6] microcracks, etc. The nonlinear ultrasound techniques make use of pulsed ultrasound waves that generate harmonic components with a higher frequency and smaller wavelengths. To accurately interpret the experimental data, a reliable and accurate numerical tool to simulate the finite-amplitude ultrasonic waves and understand the different nonlinear wave interactions becomes crucial. Moreover, an efficient numerical method in terms of memory requirements and computation time is essential to simulate the nonlinear elastic waves in a medium measuring hundreds of wavelengths and periods while maintaining a high degree of accuracy.

The most popular classes of methods for the numerical solution of full-wave problems are finite difference methods (FDM) and finite element methods (FEM), which commonly need a discretization of at least 10–20 grid points per minimum wavelength, i.e., of a maximum frequency of interest, to yield a reasonable reconstruction of the wave shape. On the other hand, integral equation methods can yield accurate results at a discretization of two grid points per minimum wavelength, i.e., at the Nyquist sampling limit.[7,8] To achieve this, an upper limit may be set on the desired spectrum of the result, and all frequencies above this limit are numerically filtered out during the intermediate steps of the computation. This approach avoids an unnecessary dense grid by removing harmonics outside of the spectrum of interest.

The iterative nonlinear contrast source (INCS) method is an integral equation method that was originally developed by Verweij *et al.*[7–12] for the modeling of the nonlinear acoustic wavefield in nonlinear, heterogeneous, and attenuating fluids. In this paper, the method will be extended to model nonlinear elastic waves and nonlinear mixing of compressional and shear waves in homogeneous, lossless, and isotropic elastic bulk media.

[a]Electronic mail: s.selvam@tudelft.nl
[b]Also at: Department of Biomedical Engineering, Erasmus University Medical Center (EMC), Rotterdam, Netherlands.

 0001-4966/2022/151(5)/3316/12/$30.00

https://doi.org/10.1121/10.0010448

Among NDT techniques, the nonlinear wave-mixing[25–27] is the most effective method in accessing the microstructural state of the material because of its flexibility to select the frequencies to be monitored, avoid measurement system nonlinearities, and choose the mixing zone location, enabling localized plastic deformation measurement. The nonlinear mixing of primary monochromatic compressional and shear waves propagating at certain frequencies, meeting the resonance conditions,[13] will generate a secondary shear wave scattered from the mixing. This secondary shear wave is also called a resonant wave[14] as the amplitude of the resonant wave grows with the increased mixing zone size of the primary pulses. In the mixing zone, an evanescent field may also be generated. This is an oscillating low amplitude elastic field with a frequency that is the sum of that of the primary waves. It does not propagate like an elastic wave, but its energy is spatially concentrated inside the mixing zone and decays over time. Jones and Kobett[13] first discussed the idea of generating a resonant wave and also proposed the necessary resonance conditions. Some literature on the application of wave-mixing in elastic media is also available. Liu *et al.*[15] developed collinear wave-mixing of elastic waves to measure the acoustic nonlinearity parameters, Chen *et al.*[14] derived a set of necessary and sufficient conditions for generating resonant waves by two propagating time-harmonic plane waves, and Tang *et al.*[6] developed a collinear wave-mixing based scanning method where the distribution of localized plastic deformation is measured. Demčenko *et al.*[16] provided the possible interactions between one longitudinal wave and two shear waves based on the analytical solution and verified by ultrasound measurements. Most of the current work[6,14,17,18] is based on one-dimensional (1D) and two-dimensional (2D) simulations using FDM and FEM. Unfortunately, these simulations do not provide a deeper understanding regarding the generation of scattered wave components and their directions, non-propagating (evanescent) waves, and the mode-converted component in the wave-mixing tests. The method described in this paper also provides physical insight into the aforementioned phenomena.

The INCS elastic method recasts a generalized form of the nonlinear elastic vector wave equation (i.e., the result of the linear momentum equation) into an integral form, which can be solved using a Neumann iterative scheme.[9] The method considers the nonlinear term of the wave equation as a distributed nonlinear contrast source in an otherwise linear background medium, and the corresponding integral equation is solved iteratively. The nonlinear contribution to the total wavefield is, thus, obtained from the nonlinear contrast source. Starting with the linear wavefield generated by the primary source (i.e., the transducer) in the background medium, the contrast source and total wavefield are iteratively updated. The result of the first iteration is the quasilinear solution. Next, the solution is iteratively improved toward the full nonlinear wavefield. As a rule of thumb, for weak to moderate nonlinearity, $j+1$ iterations suffice for accurate computation of the jth harmonic. The key step in each iteration is a spatiotemporal convolution of the distributed contrast source with the Green's function of the background medium. This is performed with the filtered convolution method,[7] which employs *a priori* filtering and fast Fourier transform (FFT) techniques to allow for a spatiotemporal grid with only two points per wavelength and period. Due to the contrast source approach[8,11] and the applied convolution technique, the INCS elastic method shows no directional dependence.

At first sight, our method seems to resemble several approaches that have been described in the literature. McCall[19] uses the Green's function to formulate an iterative scheme for computing 1D nonlinear elastic waves and derives analytical results for two very specific cases. Unlike our method, the scheme follows from perturbation analysis and contains terms with mixed orders of iteration. As a consequence, all of these orders must be stored, and the physical interpretation of the scheme is complex. Demčenko *et al.*[20] provide a general Green's function representation for the nonlinear interaction of elastic waves and apply this to compute the interaction of a propagating shear wave and an evanescent compressional wave at a fluid–solid interface. Mazilu *et al.*[21] present a plane wave method to describe the nonlinear interaction of beams with finite widths and pay explicit attention to incident evanescent waves, for which classical momentum conservation does not apply. However, both papers describe the interaction of monochromatic waves while our method can deal with the interaction of pulsed (i.e., broadband) waves that have propagated in a nonlinear fashion. To accommodate the generation and interaction of higher harmonics, our method, similar to the method of McCall, has an iterative character. In case of interacting linear waves, the method only requires one step and is in fact non-iterative.

This paper considers two numerical examples. In the first example, the modeling of a forward propagating nonlinear compressional wave in a homogeneous, isotropic, elastic medium is presented. In the second example, the modeling of nonlinear wave-mixing of compressional and shear waves is demonstrated. Also, the results of evanescent waves generated in the mixing zone of elastic waves are introduced. The literature[15,17] shows that there are three types of nonlinearity parameters (β) in elastic solids: (1) β_L is associated with the higher harmonic generation of the compressional wave, (2) β_S is associated with the higher harmonic shear waves induced by the mode conversion of the fundamental longitudinal wave into a shear wave, and (3) β_T is associated with the mixing (or interaction) of the compressional and shear waves in isotropic elastic solids with quadratic nonlinearity. These parameters are related to the Landau-Lifshitz TOE constants ($\mathcal{A}$, $\mathcal{B}$, and $\mathcal{C}$) that will be used in this paper. Using the developed approach, the generation of up to the fourth harmonic of a pulsed elastic field will be evaluated. The numerical results also demonstrate that the resonant wave can be captured efficiently. In addition, the method provides more physical insight into the wave-mixing process and explains the orientation of the scattered

fields and occurrence of non-propagating waves such as evanescent waves. The numerical solution of the evanescent waves demonstrates that the amplitudes of these waves are too small to measure experimentally.

The primary focus of this paper is an extension of the INCS method[9] for elastic waves, which will be a memory-efficient and computationally effective numerical tool for three-dimensional (3D) wave modeling in the future. The paper is structured as follows: Section II presents the theoretical background of nonlinear elastic waves in a homogeneous, isotropic, and lossless elastic medium, including basic kinematic and constitutive relations and nonlinear elastic wave equations for two different cases, as well as the modified Burgers equation for elastic waves. Section III explains the application of the INCS elastic scheme for simulating the presented cases. In Sec. IV, the numerical results obtained with the INCS elastic method for the modeling of a pure compressional wave and its comparison with the benchmark solution, the modeling of mixing of compressional and shear waves, and its comparison with the published literature results are shown. Furthermore, the capability of the method to model an evanescent wave generated by wave-mixing and its non-propagating properties are explained. Section V discusses the numerical challenges involved in the proposed method and its ability to predict the evanescent components. The last section, Sec. VI concludes by discussing the extension of the INCS method to elastic waves and its key features.

II. THEORETICAL FRAMEWORK

Within the framework of continuum mechanics, the nonlinear kinematic and constitutive relations[1,22] between the field quantities are usually expressed in a Lagrangian description of motion in which the initial configuration (X_i) and deformed configuration (x_i) of the medium are not same.

A. Basic kinematics and constitutive relation

Deformation of a continuum body results in a displacement of the material particles, u_i. The deformation results in a strain, and the most useful measure of strain in finite deformations is the Green-Lagrangian strain, E_{ij}. The kinematic relation between the strain and displacement of the particles is expressed in index notation as[1]

$$E_{ij} = \frac{1}{2}\left(\frac{\partial u_i}{\partial X_j} + \frac{\partial u_j}{\partial X_i} + \frac{\partial u_k}{\partial X_i}\frac{\partial u_k}{\partial X_j}\right), \tag{1}$$

where X_i denotes the particle position in the reference (or initial) configuration. In large deformations (e.g., in the case of high field values in nonlinear elastics), the useful stress measure is the second Piola-Kirchoff stress, S_{ik}, that is related to the Green-Lagrangian strain through the strain energy function W as shown below.[1] The second-Piola-Kirchoff stress is defined as

$$S_{ik} = \frac{\partial W}{\partial E_{ik}}. \tag{2}$$

Using the summation convention, the general form of the strain energy function in a nonlinear elastic medium is given by

$$W = \frac{1}{2}C_{ijkl}E_{ij}E_{kl} + \frac{1}{3!}C_{ijklmn}E_{ij}E_{kl}E_{mn} + \cdots, \tag{3}$$

where C_{ijkl} and C_{ijklmn} are second-order and TOE moduli. For an isotropic material, the strain energy function has the form

$$W = \frac{\lambda}{2}(\mathrm{tr}\,E)^2 + \mu\,\mathrm{tr}(E^2) + \frac{\mathcal{C}}{3}(\mathrm{tr}\,E)^3 + \mathcal{B}\,(\mathrm{tr}\,E)\mathrm{tr}\,E^2 + \frac{\mathcal{A}}{3}\mathrm{tr}\,E^3, \tag{4}$$

where $\mathrm{tr}\,E = E_{ii}$ is the trace of E_{ij}. Using the above energy function and considering up to second-order terms in the displacement, the general constitutive relation between the second Piola-Kirchoff stress tensor and the Green-Lagrangian strain tensor can be written as

$$\begin{aligned} S_{ik} &= \lambda\,\mathrm{tr}\,E\delta_{ik} + 2\,\mu E_{ik} + \mathcal{C}(\mathrm{tr}\,E)^2\delta_{ik} \\ &\quad + \mathcal{B}\left[2E_{ik}(\mathrm{tr}\,E) + \mathrm{tr}\,E^2\delta_{ik}\right] + \mathcal{A}E_{ik}^2. \end{aligned} \tag{5}$$

Here, λ and μ are the Lamé constants and $\mathcal{A}$, $\mathcal{B}$, and $\mathcal{C}$ are TOE constants.

B. Nonlinear elastic wave equation

To derive the nonlinear elastic wave equation, we start with the balance of momentum,

$$\partial_j P_{ij} + f_i^{\mathrm{pr}} = \rho_0 \partial_t^2 u_i, \tag{6}$$

where P_{ij} represents the first Piola-Kirchoff stress tensor, which is related to S_{ij}, and the term f_i^{pr} represents the source that excites the wave in the medium, and ρ_0 is the density of the undeformed medium. The spatial derivatives are with respect to the X_i coordinate. The general form of the nonlinear elastic vector wave equation can be obtained by expanding P_{ij} using S_{ij} and writing everything in terms of u_i, yielding

$$\rho_0\,\partial_t^2 u_i - (\lambda+\mu)\,\partial_i\partial_k u_k - \mu\,\partial_k\partial_k u_i = f_i^{\mathrm{pr}} + f_i^{\mathrm{nl}}, \tag{7}$$

where f_i^{nl} is the nonlinear force or contrast source term that accounts for the material nonlinearity of the medium considered up to quadratic terms in the displacement. It can be expressed as

$$\begin{aligned} f_i^{\mathrm{nl}} &= C_1\left[(\partial_k^2 u_m)(\partial_i u_m) + (\partial_k^2 u_m)(\partial_m u_i)\right. \\ &\quad \left. + 2(\partial_m\partial_k u_i)(\partial_k u_m)\right] + C_2\left[(\partial_i\partial_k u_m)(\partial_k u_m)\right. \\ &\quad \left. + (\partial_m\partial_k u_k)(\partial_m u_i)\right] + C_3\left[(\partial_k^2 u_i)(\partial_m u_m)\right] \\ &\quad + C_4\left[(\partial_m\partial_k u_k)(\partial_i u_m) + (\partial_i\partial_k u_m)(\partial_m u_k)\right] \\ &\quad + C_5\left[(\partial_i\partial_k u_k)(\partial_m u_m)\right], \end{aligned} \tag{8}$$

where the coefficients are given as

https://doi.org/10.1121/10.0010448

$$C_1 = \mu + \frac{\mathcal{A}}{4}, \tag{9}$$

$$C_2 = \lambda + \mu + \frac{\mathcal{A}}{4} + \mathcal{B}, \tag{10}$$

$$C_3 = \lambda + \mathcal{B}, \tag{11}$$

$$C_4 = \frac{\mathcal{A}}{4} + \mathcal{B}, \tag{12}$$

$$C_5 = \mathcal{B} + 2\mathcal{C}. \tag{13}$$

1. Wave equation for purely compressional wave

As a first simplified case, we assume that the wave propagates along the x-direction only, and the particle motion is parallel to the direction of propagation, i.e., we consider a plane compressional wave. The governing nonlinear elastic wave equation in a homogeneous, lossless, isotropic elastic medium is, in this case, given as

$$\rho_0 \frac{\partial^2 u_x}{\partial t^2} - (\lambda + 2\mu)\frac{\partial^2 u_x}{\partial x^2} = f_x^{\mathrm{pr}} + f_x^{\mathrm{nl}}. \tag{14}$$

Here, the summation convention has not been applied. The expression for the nonlinear contrast source, f^{nl}, now becomes

$$f_x^{\mathrm{nl}} = [c_1 + c_2]\frac{\partial u_x}{\partial x}\frac{\partial^2 u_x}{\partial x^2}, \tag{15}$$

where $c_1 = 3(\lambda + 2\mu)$ and $c_2 = 2\mathcal{A} + 6\mathcal{B} + 2\mathcal{C}$. The nonlinear force term, f^{nl}, accounts for the higher harmonic generation through the multiplication of the field with itself and is also called self-mixing or auto-convolution in some literature.

2. Modified Burgers equation for purely compressional wave

We employ a numerical solution of the modified Burgers equation[9,23] for purely compressional wave propagation as a benchmark solution for the INCS results. Starting from a source-free version of the nonlinear elastic wave equation (14), the modified Burgers equation is obtained in terms of particle velocity, $v = \partial u/\partial t$, as

$$\frac{\partial v}{\partial x} = \frac{\beta}{c_p^2} v \frac{\partial v}{\partial \tau}, \tag{16}$$

where c_p is the compressional wave speed, and

$$\beta = \left(\frac{3}{2} + \frac{2\mathcal{A} + 6\mathcal{B} + 2\mathcal{C}}{2(\lambda + 2\mu)}\right) \tag{17}$$

is the coefficient of nonlinearity of the compressional wave. The variable, $\tau = t - x/c_p$, represents the co-moving or retarded time variabe that travels along with the wave. Within the co-moving time frame, the variation of the wavefield with respect to x is small. Using the implicit solution[9] available for such a differential equation, the nonlinear particle displacement can be obtained.

3. Mixing of compressional and shear waves

As a second simplified case, we consider two primary plane waves propagating collinearly in the same direction (one-way mixing) and opposite directions (two-way mixing) in a homogeneous, isotropic nonlinear elastic solid.[14] We assume that both waves are propagating in the x-direction. Let u_x and u_y be the displacement components of the primary compressional and shear waves, respectively. The governing nonlinear partial differential equation of the compressional wave is

$$\rho_o \frac{\partial^2 u_x}{\partial t^2} - (\lambda + 2\mu)\frac{\partial^2 u_x}{\partial x^2} = f_x^{\mathrm{pr}} + f_x^{\mathrm{nl}}, \tag{18}$$

where the contrast source compressional component, f_x^{nl}, is

$$f_x^{\mathrm{nl}} = [c_1 + c_2]\frac{\partial u_x}{\partial x}\frac{\partial^2 u_x}{\partial x^2} + c_3\frac{\partial u_y}{\partial x}\frac{\partial^2 u_y}{\partial x^2}, \tag{19}$$

in which

$$c_3 = \left(\lambda + 2\mu + \frac{\mathcal{A}}{2} + \mathcal{B}\right). \tag{20}$$

In Eq. (19), the first term in f_x^{nl} represents the higher harmonic generation of the compressional wave, and the second term represents the mode conversion of shear waves into compressional waves. The corresponding nonlinear partial differential equation of the shear wave is

$$\rho_0 \frac{\partial^2 u_y}{\partial t^2} - \mu\frac{\partial^2 u_y}{\partial x^2} = f_y^{\mathrm{pr}} + f_y^{\mathrm{nl}}, \tag{21}$$

where the contrast source shear component, f_y^{nl}, is

$$f_y^{\mathrm{nl}} = c_3\left(\frac{\partial u_x}{\partial x}\frac{\partial^2 u_y}{\partial x^2} + \frac{\partial u_y}{\partial x}\frac{\partial^2 u_x}{\partial x^2}\right). \tag{22}$$

The terms in Eq. (22), represent the mixing of compressional (u_x) and shear (u_y) waves. Several works in the literature show that when primary compressional and shear waves mix at a certain frequency and satisfy the resonant conditions[13,16] inside an elastic medium, the secondary resonant wave will be generated at a specific resonant frequency and, indeed, propagate at the shear wave velocity. In general, the amplitude of this resonant wave depends on the size of the mixing zone and number of cycles of the primary waves. The mixing zone location[6] can be modified by setting a time-delay in the primary source functions.

III. NEUMANN ITERATIVE SCHEME AND EFFICIENT DISCRETIZATION

The nonlinear partial differential equations (14), (18), and (21) can be expressed in the integral form[16]

$$u(x,t) = \frac{1}{\rho_0 c_0^2} \int_{t'=t_0=0}^{T} \int_{x' \in D} G(x-x', t-t') \times \left[f^{\mathrm{pr}}(x',t') + f^{\mathrm{nl}}(x',t') \right] dx' dt' \tag{23}$$

$$= \frac{1}{\rho_0 c_0^2} G *_{x,t} (f^{\mathrm{pr}} + f^{\mathrm{nl}}(u)), \tag{24}$$

where c_0 is the relevant wave speed at hand (compressional wave speed, c_p, or shear wave speed, c_s), and T and D are the temporal and spatial supports of the involved sources, respectively. Function G is the Green's function of the corresponding linear "background" medium, which corresponds to the left-hand side of the wave equation. Equation (24) gives an implicit solution for the relevant particle displacement because the contrast source term, $f^{\mathrm{nl}}(x',t') = f^{\mathrm{nl}}(u)$, depends on the particle displacement as well. Equations (23) and (24) represent the convolution between the Green's function of the linear background medium and source terms over all of the spatiotemporal dimensions. The 1D Green's function[9] of the linear background medium is given by

$$G(x,t) = \frac{c_0}{2} H\left(t - \frac{|x|}{c_0} \right), \tag{25}$$

where H is the Heaviside step function.

Increasingly accurate approximations to the explicit solution of the convolution equation (24) can be obtained using the Neumann iterative scheme,

$$u^{(j)} = G *_{x,t} \left[f^{\mathrm{pr}} + f^{\mathrm{nl}}(u^{(j-1)}) \right], \tag{26}$$

in which the nonlinear displacement field, u^j, is a summation of the linear field solution, $u^{(0)}$, and a nonlinear field correction, $\delta u^{(j)}$. The iterative scheme is explained graphically in Fig. 1. The iterative scheme contains two major blocks of operations: the updating source and updating field. In iteration $j=0$, only the given source, $f^0 = f^{\mathrm{pr}}$, is involved, and the linear displacement field, $u^{(0)}$, is obtained by convolving the Green's function and primary source over the entire spatiotemporal support of this source. Once the linear field is obtained, j is incremented, and the linear field is substituted in the equation of the relevant nonlinear contrast source [Eqs. (15), (19), and (22)] to obtain the contrast source $f^{(1)} = f^{\mathrm{nl}}(u^{(0)})$. Now the iteration continues with calculating the first nonlinear correction, $\delta u^{(1)} = G *_{x,t} f^1$, resulting in the first nonlinear field estimate $u^{(1)} = u^{(0)} + \delta u^{(1)}$. The iteration continues by setting $j = j+1$ and proceeding in the same manner to yield the next nonlinear displacement correction. The convolution is performed in the wavenumber-frequency domain, in which the convolution operation becomes the multiplication of their respective Fourier coefficients. In this way, the convolution can be performed with minimum computational effort and a coarse grid. To achieve this, all of the relevant quantities are spatially and temporally filtered and windowed before the convolution step, as explained in detail by Verweij and Huijssen.[7]

During the evaluation of the contrast source, the multiplication of the first-order and second-order derivatives of the band limited displacement fields results in a spectrum with an increased bandwidth. Before this step, the sampling intervals must be reduced by a factor of 2 in each spatiotemporal dimension to avoid aliasing errors. This can be achieved by, first, zero padding the samples in the Fourier domain and then transforming back into the original domain, giving interpolated samples in the original domain without affecting its spectral content, after which the multiplication may take place. The spectrum of the obtained contrast source results may exceed the original Nyquist frequency and has to be numerically filtered in the Fourier domain to limit the spectrum and obtain the original sample size. The entire numerical procedure for the interpolation and filtering operations is outlined in Verweij and Huijssen.[7]

IV. NUMERICAL MODEL AND RESULTS

In this section, the 1D numerical results for the considered numerical examples, as obtained by the INCS elastic method, are presented.

A. Harmonic generation of pure compressional wave

1. Primary source

In the first example, we consider the nonlinear propagation of a pure compressional plane wave excited by a plane source, f^{pr} [Nm^{-3}], representing the density of the external force acting at $x=0$. The excited wave is propagating in the positive x-direction up to a certain distance $X = 5\,\mathrm{cm}$ and a maximum time $T = 10\ \mu\mathrm{s}$ in a 1D elastic medium. The primary source function acting as a pulsed excitation is represented as

$$f^{\mathrm{pr}} = 2Q_0 s(t) \delta(x), \tag{27}$$

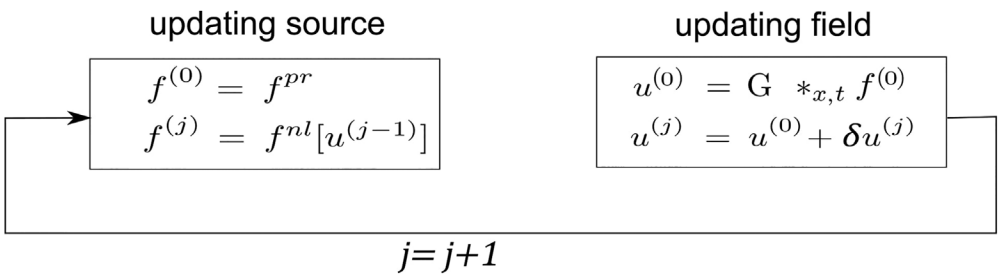

FIG. 1. The Neumann iterative scheme.

https://doi.org/10.1121/10.0010448

TABLE I. The material properties of aluminum.

ρ	c_p	c_s	λ	μ	$\mathcal{A}$	$\mathcal{B}$	$\mathcal{C}$
2700 kg/m^3	6198 m/s	3122 m/s	51.1 GPa	26.3 GPa	−282 GPa	−179 GPa	53 GPa

where $Q_0 = 5$ MPa is the source amplitude in terms of the applied stress, $\delta(x)$ denotes a delta pulse acting at $x = 0$, and $s(t)$ is the source signature representing a harmonic time signal with a Gaussian envelope,

$$s(t) = \exp\left[-\left(\frac{t - T_d}{T_w/2}\right)^2\right] \sin\left[2\pi f_0 (t - T_d)\right], \tag{28}$$

where $T_w = 6/f_0$ and $T_d = 3/f_0$ are the width and delay of the envelope (so it is still negligible for $t = 0$), respectively, and $f_0 = 5$ MHz is the chosen fundamental frequency. We are interested in the frequency content of the wavefield up to the fourth harmonic and, therefore, the maximum frequency of interest is taken as $F_{\text{nyq}} = 4.5 f_0$. The considered medium is aluminum, and the material properties are shown in Table I.[14]

In INCS, the temporal angular cut-off frequency, $\Omega = 2\pi F_{\text{nyq}}$, is the prime parameter determining the spatial and temporal discretizations. The required sampling frequency for the given Nyquist sampling limit is $F_s = 2F_{\text{nyq}}$.[9] The corresponding spatial cut-off frequency, K, can be evaluated as $K = \Omega/c_0$. As a result of the applied temporal and spatial filtering, the time domain discretization steps are taken as $\delta t = \pi/\Omega$ and $\delta x = \pi/K$.[7]

2. Simulation results

In the first numerical example, pulsed compressional wave propagation in an infinite homogeneous, isotropic, nonlinear elastic medium is considered. The material nonlinearity results in the distortion of the input field that accumulates along the propagation path such that the contrast source can be assumed to lie in the region between the primary source location and the observation point. The nonlinear distortion that accounts for the second and higher harmonic generations of the wavefield grows with an increasing propagation distance. The grid point at the end of the domain is taken as the observation point. The nonlinearly distorted signal can be seen clearly through the generation of harmonics in the frequency domain plots in Fig. 2. Figure 2 shows the spectrum of the nonlinear displacement

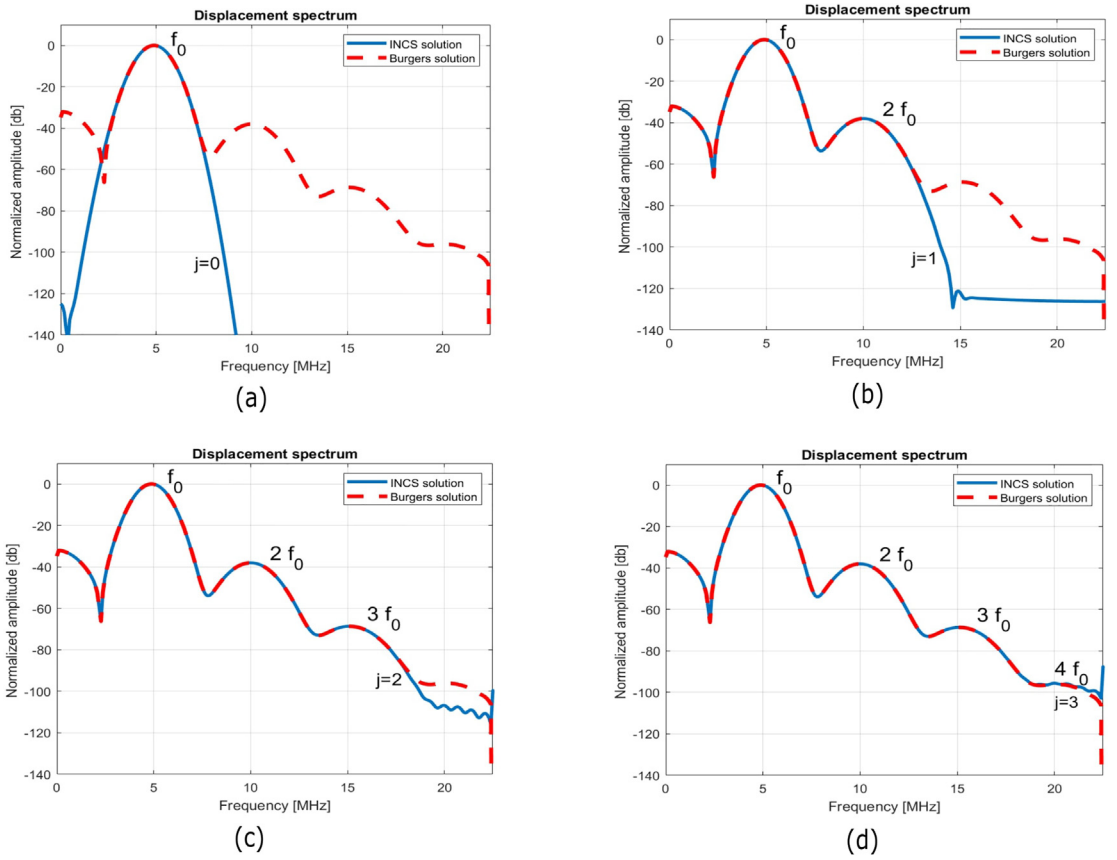

FIG. 2. (Color online) The spectra of the nonlinear displacement field ($u^{(j)}$) for iterations $j = 0$ to $j = 3$, yielding the fundamental up to the fourth harmonic. The maximum of the spectrum is the Nyquist frequency, $F_{\text{nyq}} = 4.5 f_0 = 22.5$ MHz.

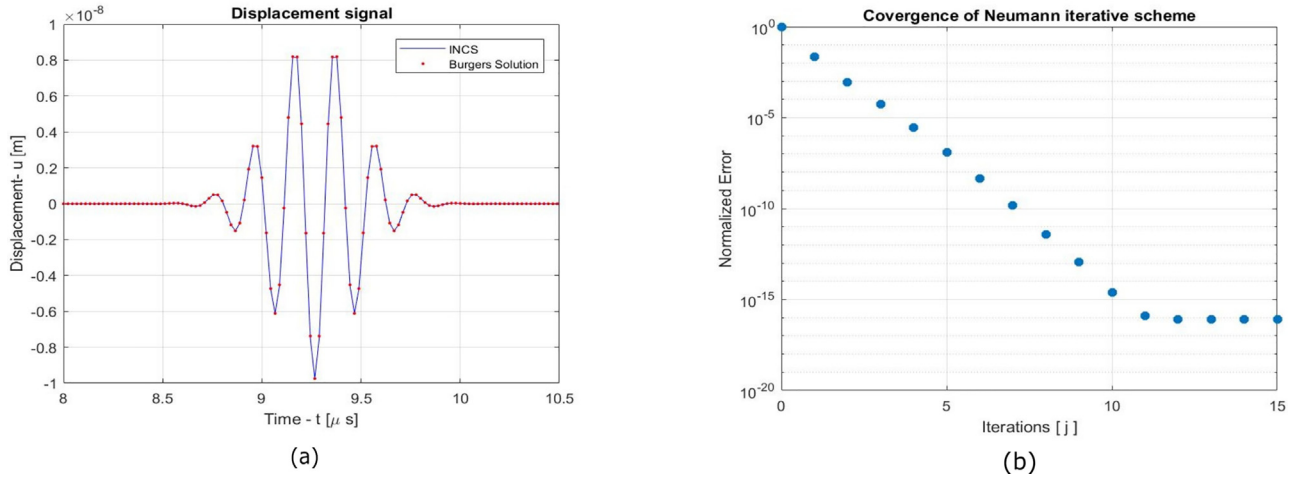

FIG. 3. (Color online) The (a) nonlinear displacement ($u^{(j)}$) obtained using the INCS elastic method with $j = 3$ (solid) and the modified Burgers solution (red dotted) at $x = 5$ cm is shown as well as the (b) normalized error showing the convergence of the Neumann iterative scheme.

field up to three iterations. The plots clearly show the buildup of the harmonics during the iteration process. In each iteration, the source field is updated with the field of the new contrast source to yield increasingly higher harmonics.

In Fig. 2, we observe that each iteration shows a better approximation with the reference solution (modified Burgers solution) for increasingly higher iterations. The normalized amplitude is obtained in decibels by normalizing the spectrum with its maximum value. At the maximum frequency, $F_{\text{nyq}} = 4.5f_0 = 22.5$ MHz, the spectrum of the excitation pulse is 100 dB below the level of the center frequency. The time domain field at the maximum propagated distance and iteration $j = 3$ is shown in the Fig. 3(a). The solution obtained using the INCS elastic method is in good agreement with modified Burgers solution with a maximum difference of below -0.04 dB for the first three harmonics.

3. Convergence of the Neumann iterative scheme

The numerical convergence of the Neumann iterative scheme toward a steady solution of the computed field is demonstrated using the error function, ERR$^{(j)}$,[11,12] defined as

$$\text{Err}^{(j)} = \frac{\|u^{(j-1)} - u^{(j)}\|}{\|u^{(0)}\|}. \tag{29}$$

The normalized error value of the obtained field solution for 15 iterations is shown in Fig. 3(b). As can be seen in Fig. 3(b), the error, ERR$^{(j)}$, steadily decreases for increasing j, thus, the obtained solution converges toward a steady solution. The convergence of the solution is achieved after 12 iterations, where ERR$^{(j)} \approx 10^{-16}$, which is related to the numerical precision of the computer. For the medium considering stronger nonlinearities, a greater number of iterations or a different iterative scheme could be required.

B. Mixing of compressional and shear waves

In the second numerical example, the collinear mixing of two pulsed waves, one nonlinear compressional wave and one nonlinear shear wave, is considered.[14,15] Figure 4 illustrates the mixing process. When two sources are excited at the same location, it is called one-way mixing; conversely, when the sources are excited at opposite ends of the medium, it is called two-way mixing. The area marked in red denotes the mixing zone inside the medium. The amplitude of the resultant resonant wave generated from the mixing depends on the mixing zone size, which can be adjusted by changing the number of load cycles in the input signals.

The obtained 1D results from the INCS elastic method are compared with the published results[14] using FEM. The purpose of conducting this numerical test is to determine the capability of the INCS elastic method to accurately

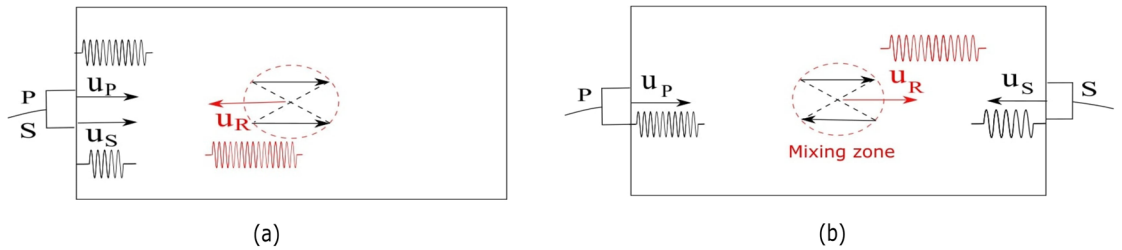

FIG. 4. (Color online) The (a) one-way wave-mixing and (b) two-way wave-mixing.

https://doi.org/10.1121/10.0010448

simulate nonlinear wave-mixing of elastic waves and capture the resonant wave and, also, to get more insight into the mixing mechanisms.

1. Primary sources

We consider the pulsed propagation of compressional and shear waves in a homogeneous, isotropic, nonlinear elastic medium. The material properties are the same as those listed in Table I. The maximum propagation distance is taken as $X_{\max} = 7.2\,\text{cm}$ and a maximum time is $T = 32\ \mu\text{s}$. The labels p, s, and r will be used to denote the primary compressional, primary shear, and mixed resonant waves, respectively.

The primary source functions of the compressional and shear waves are represented as

$$f_p^{\text{pr}} = \begin{cases} \sigma_p \sin(2\pi f_p t)\,\delta(x) & \text{if } 0 \le t \le N_p/f_p, \\ 0 & \text{otherwise}, \end{cases} \tag{30}$$

$$f_s^{\text{pr}} = \begin{cases} \sigma_s \sin(2\pi f_s t)\,\delta(x) & \text{if } 0 \le t \le N_s/f_s, \\ 0 & \text{otherwise}, \end{cases} \tag{31}$$

respectively. The spatial length of the signals can be controlled by the number of load cycles and determines the size of the mixing zone. The INCS simulations are conducted using the input source parameters chosen from the literature[14] and listed in the Table II. The ten cycles of compressional pulses and five cycles of shear pulses are chosen to yield the same spatial length of the primary sources. The source amplitudes are implemented in terms of applied stresses (σ_p, σ_s), and the corresponding displacements are $u_p = 1 \times 10^{-8}$ m for the compressional source and $u_s = 1 \times 10^{-7}$ m for the shear source.

2. One-way mixing

In this section, we will analyze the collinear mixing of pulsed time-harmonic compressional and shear waves, both propagating collinearly in the $+x$ direction. In one-way mixing, illustrated in Fig. 4(a), the two sources are excited at the same location, $x = 0$, and propagate forward. Forward propagation from $x = 0$ to $X_{\max}$ is denoted by "+"; backward propagation from $x = X_{\max}$ to 0 is denoted by "−" here. A delay of 8 μs is applied to the compressional wave to enable the mixing of primary waves at the center of the medium. The wave-mixing is a nonlinear phenomenon, and the shear term of the contrast source, f_y^{nl}, represents this nonlinear interaction process. Analyzing this contrast source in the wavenumber-frequency (k, ω) domain will offer a physical understanding of the generation of the mixing products.

The mixing of two waves at different frequencies ($f_p = 10$ MHz, $f_s = 7.5$ MHz) results in the generation of a wavefield with two different frequency components, i.e., the sum ($f = 17.5$ MHz) and their difference ($f = 2.5$ MHz). Figure 5(a) shows the (k, ω) domain plot of the contrast source, f_y^{nl}. The (k, ω) domain representation of the shear wave Green's function, $\hat{G}_s$, is also shown by the dashed yellow line. It can be clearly seen that the line of the shear Green's function crosses the low frequency part of the contrast source at $f = 2.5$ MHz. This should be interpreted as the mixing or resonant shear wave, $\hat{u}_y^{r-}$, as shown in Fig. 5(b) computed with the $j = 1$ iteration. The frequency component at $f_e = 17.5$ MHz is not crossed by the line of the Green's function and should be interpreted as an evanescent wave that does not propagate out of the mixing zone and attenuates over time. The presence of a resonant component with a negative wavenumber indicates the backward propagation of the resonant wave, $\hat{u}_y^{r-}$. The combination of the wavenumber and frequency shows that this component travels at the shear wave speed, c_s.

The resonant field is transformed back to the (x,t) domain. The backward propagating resonant wave, $\hat{u}_y^{r-}$, as received at $x = 0$ is shown in Fig. 6, in which both the INCS and reference solution from the literature[14] are plotted together. The frequency spectrum at this location is presented in Fig. 6 and shows a peak at the resonant frequency ($f_r = 2.5$ MHz).

3. Two-way mixing

As illustrated in Fig. 4(b), in the two-way mixing test, the primary sources are excited at the opposite ends of the medium. A pulsed compressional wave is generated at $x = 0$ and propagates in the forward direction, and a pulsed shear wave is generated at $x = X_{\max}$ and propagates in the backward direction.

Similar to the one-way mixing case, the (k, ω) domain plot of the contrast source shear term, f_y^{nl}, in the two-way mixing process is computed, requiring $j = 1$ iteration, and shown in Fig. 7(a). The mixing of the primary waves ($f_p = 10$ MHz, $f_s = 2.5$ MHz) generates the resonant shear component at frequency $f_r = 7.5$ MHz because it overlaps with the shear Green's function. The resulting resonant component in Fig. 7(a) has a positive wavenumber, which indicates the forward propagation of the resonant wave, $\hat{u}_y^{r+}$. The combination of the wavenumber and frequency shows that this component travels at shear wave speed (c_s).

TABLE II. The primary source parameters as used in the wave-mixing simulations.

Source	Type of mixing	Amplitude (MPa)	Frequency (MHz)	Number of cycles	Pulse length (mm)
Compressional	One-way	$\sigma_p = 10.85$	$f_p = 10$	$N_p = 10$	$L_p = 6.2$
	Two-way				
Shear	One-way	$\sigma_s = 42.3$	$f_s = 7.5$	$N_s = 5$	$L_s = 6.2$
	Two-way	$\sigma_s = 13.2$	$f_s = 2.5$		

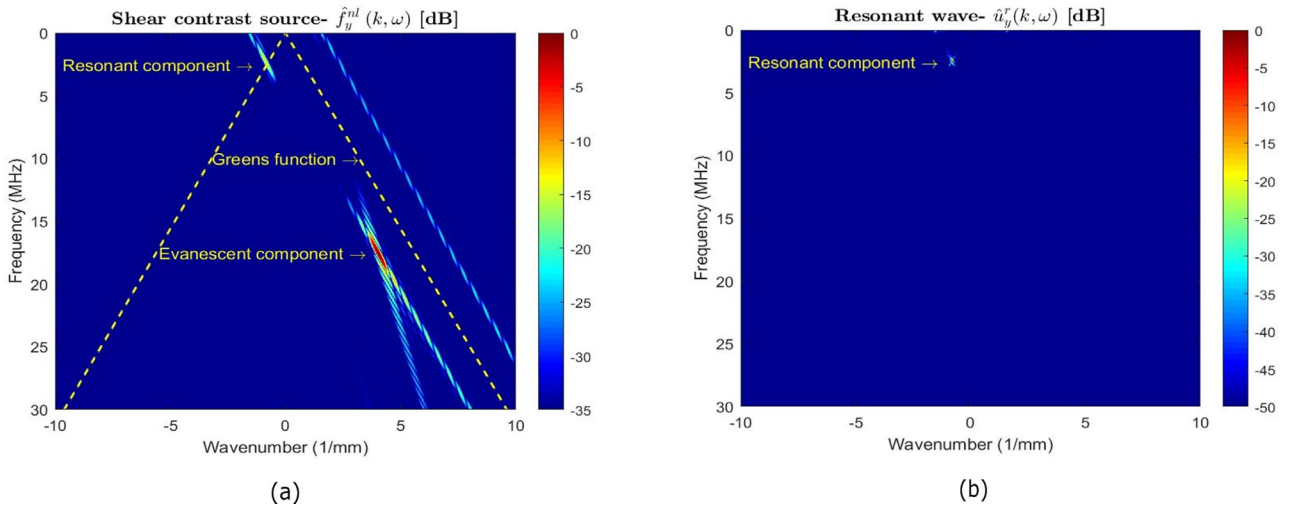

FIG. 5. (Color online) One-way mixing in the (k,ω) domain depicted by the (a) nonlinear shear contrast source, $\hat{f}_y^{\mathrm{nl}}(k,\omega)$. The 0 dB level corresponds to a force of $f_y^{\mathrm{nl}} = 7.15 \times 10^8$ N/m^3. (b) The resonant wave, $\hat{u}_y^r(k,\omega)$ with the 0 dB level corresponding to a displacement of $u_y^r = 3.23 \times 10^{-7}$ mm.

Clearly, the analysis of the nonlinear shear contrast source in the (k,ω) domain explains the wave-mixing process in terms of the generated frequency components, propagating and non-propagating waves, and the orientations of the scattered waves.

The forward propagating resonant wave, u_y^{r+}, is received at $x = X_{\max}$ and the corresponding time domain waveform and normalized frequency spectra with a peak at $f_r = 7.5$ MHz are shown in Fig. 8, in which the reference solution from the literature[14] is also shown.

The resonant wavefields obtained with the INCS elastic method in the one-way and two-way mixing cases are quantitatively compared with the results published in the literature.[14] We compared the time domain amplitude peaks of the resonant wave displacement between the INCS results (Figs. 6 and 8) and published results[14] by calculating the root mean square (RMS) error and scatter index (SI), which are given by

$$\text{RMS error} = \sqrt{\frac{\sum_{p=1}^{N} (u_I - u_P)^2}{N}}, \tag{32}$$

$$\text{SI} = \frac{\text{RMS error}}{\text{mean}(u_P)} \times 100, \tag{33}$$

respectively, where N is the number of time domain peaks, u_I and u_P are the resonant wave displacement values of the INCS and published results, respectively, and SI gives the percentage of the RMS error difference with respect to the reference solution. The RMS error for the one-way mixing is calculated to be 1.63×10^{-11}, which gives the SI value of 7.38%, and for the two-way mixing, the RMS error is 1.46×10^{-11}, which gives the SI value of 6.8%. This shows a good agreement of the INCS results with the published results. Also, the obtained results show an excellent

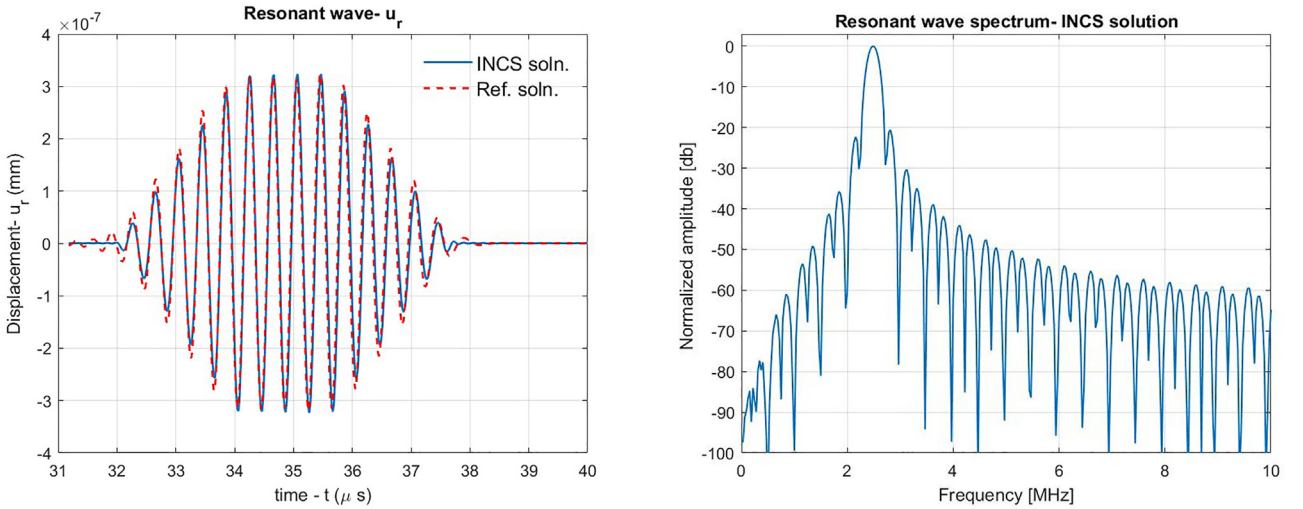

FIG. 6. (Color online) One-way mixing depicted by the (a) time domain plot of the resonant wave u_y^r (blue solid line, INCS solution; red dash, reference solution) and (b) corresponding frequency spectrum, $\hat{u}_y^r$.

https://doi.org/10.1121/10.0010448

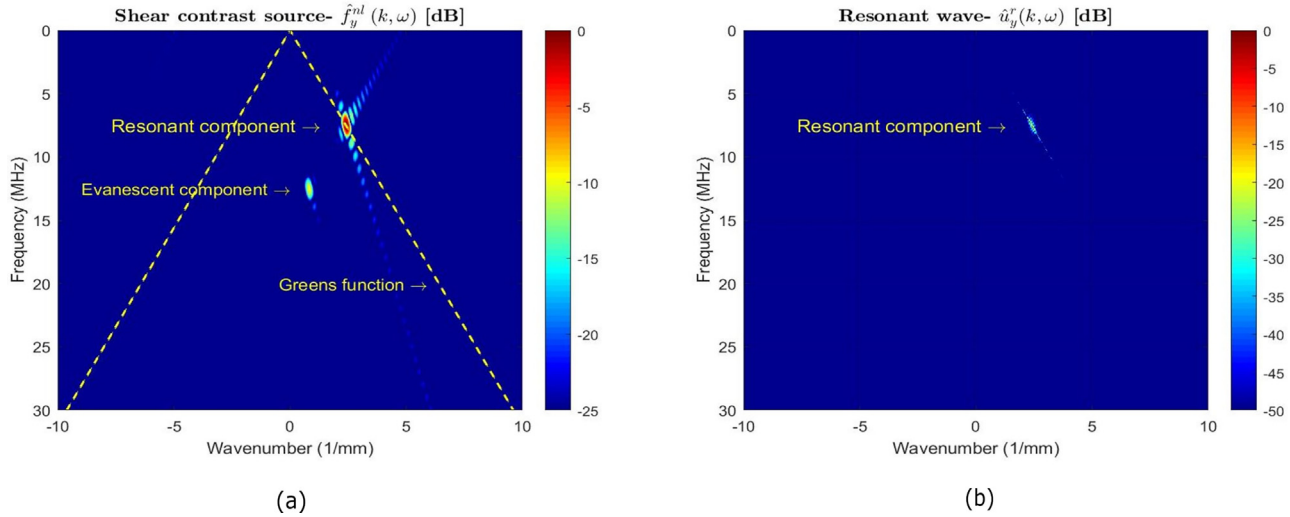

FIG. 7. (Color online) Two-way mixing in the (k,ω) domain depicted by the (a) nonlinear shear contrast source, $\hat{f}_y^{\mathrm{nl}}(k,\omega)$. The 0 dB level corresponds to a force of $f_y^{\mathrm{nl}} = 2.82 \times 10^8$ N/m^3, (b) The resonant wave, $\hat{u}_y^r(k,\omega)$ with the 0 dB level corresponding to a displacement of $u_y^r = 3.2 \times 10^{-7}$ mm.

agreement in terms of other physical characteristics of the resonant wavefield, such as the pulse shape, resonant frequency, and number of cycles. The simulation results demonstrate the capability of the INCS elastic method to accurately capture the resonant wave at a coarse discretization of two grid points per minimum wavelength and further provide more physical insight into the nonlinear wave-mixing process.

V. DISCUSSION

In this section, numerical challenges involved in the proposed method and its ability to predict the evanescent components are discussed.

In the first numerical example, the presented comparison between the INCS elastic method and modified Burgers solution confirms that the proposed method reproduces the nonlinear displacement field accurately up to the fourth harmonic. In agreement with the earlier investigations by the authors of the original INCS,[7–12] the example has confirmed that for the accurate computation of the hth harmonic, the maximum Nyquist frequency can be set at $F_{\mathrm{nyq}} = (h+0.5)f_0$ and taking the iteration $j = h+1$ is already sufficient.

Much attention is given to the evaluation of the contrast source, f^{nl}. The spatial derivatives of the wavefield introduce numerical artifacts at the domain boundaries such that the medium is extended with sufficient grid points at both ends. The contrast source must be numerically interpolated and filtered in spatiotemporal dimensions to avoid the aliasing error due to the increased bandwidth in the multiplication operation,[7] but the spatial filtering step has been skipped, just as in the original method.[8]

For the implementation of the primary sources, a finite number of cycles of sine pulses are chosen. The Fourier domain representation of such input pulses (i.e., a sinc function centered around the frequency of the sine) together with

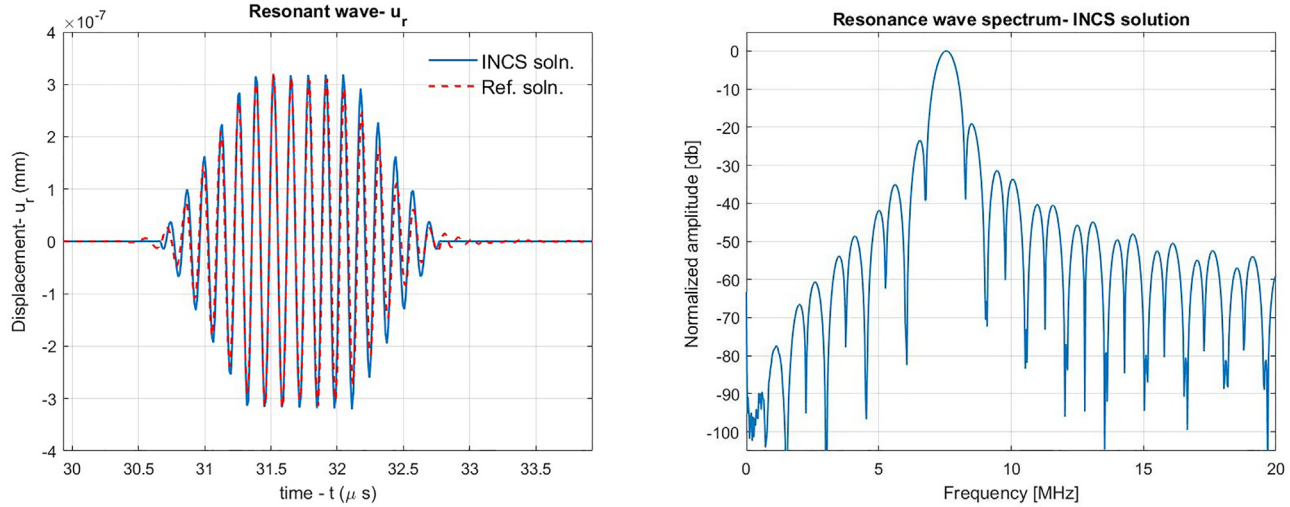

FIG. 8. (Color online) Two-way mixing depicted by the (a) time domain plot of the resonant wave, u_y^r (blue solid line, INCS solution; red dash, reference solution) and (b) corresponding frequency spectrum, $\hat{u}_y^r$.

the singularity in the 1D Green's function will produce a strong DC offset (i.e. deviation of the mean amplitude from zero) at zero wavenumber and yield an incorrect displacement. The reason for this error is that a force should act in two directions in view of Newton's third law. To account for this, equal and opposite forces are applied at the source locations, where both forces cause waves propagating away from the source in the opposite directions. This will balance the forces spatially and, thus, results in a correct displacement solution.

As an additional advantage, the method provides control over the spectral content of the field quantities during intermediate steps, providing the flexibility to numerically evaluate the non-propagating components of the mixing, i.e., evanescent wave, by applying high-pass filtering. From Figs. 5(a) and 7(a), it is evident that the resonant frequency component can be numerically filtered out in the (k, ω) domain, resulting in the nonlinear shear contrast source, f_y^{nl}, with only the evanescent field contribution. The field of contrast source can then be computed by multiplication with the shear Green's function and transformed back to the (x, t) domain. The numerical result of the evanescent wave in the two-way mixing process is shown in Fig. 9. The same procedure can be applied to the one-way mixing process.

In a same manner, another non-propagating component, i.e., the mode-converted shear term that appears in the contrast source compressional term f_x^{nl} in Eq. (19), can also be evaluated. The maximum amplitude of the computed evanescent wave is 1.25×10^{-12} m, i.e., 98 dB smaller than the shear source amplitude. The numerical results show that the evanescent wave is difficult to measure when generated inside a bulk medium at any substantial propagation distance in the setup of our interest.

In case of an anisotropic, inhomogeneous elastic medium with attenuation, the additional effects can be modeled by including them as extra contrast source terms on the right-hand side of the wave equation (7). For such media, the influence of the additional contrast sources may be large compared to the quadratic nonlinearity source alone, therefore, the Neuman iterative scheme may converge slowly or not at all. This will require the application of advanced iterative schemes, such as over-relaxation methods or conjugate gradient (CG) methods, to solve the integral equations.[10,12,24]

VI. CONCLUSIONS

The key purpose of this paper has been to extend the INCS method to the elastic case and demonstrate the applicability of this INCS elastic method to simulate the generation of higher harmonics and the nonlinear wave-mixing of elastic waves. The numerical results presented for the 1D-pulsed compressional wave show an excellent agreement with the reference solution obtained using the modified Burgers equation. The presented results for the resonant wave generated in the collinear mixing (one-way and two-way) of compressional and shear waves in a nonlinear elastic medium show a good agreement with the published results.[14] Further, it has been explained that the resulting components from the wave-mixing process, their orientations, and their propagating or evanescent behaviors directly follow from the (k, ω) domain representation of the nonlinear contrast source, which plays a key role in this method. The nonlinear force components represented by this contrast source can be evaluated separately and enable one to independently simulate and study the waves that are caused by the various physical phenomena that arise.

The numerical results obtained with the INCS elastic method may provide useful information to design an ultrasound measurement setup to conduct a wave-mixing experiment and measure the resonant wave amplitude in a solid material, which is further useful in accessing the nonlinearity parameters and microscopic material properties. In addition, the numerical predictions show that the evanescent waves generated inside an elastic material are difficult to measure from the surface. The promising results motivate

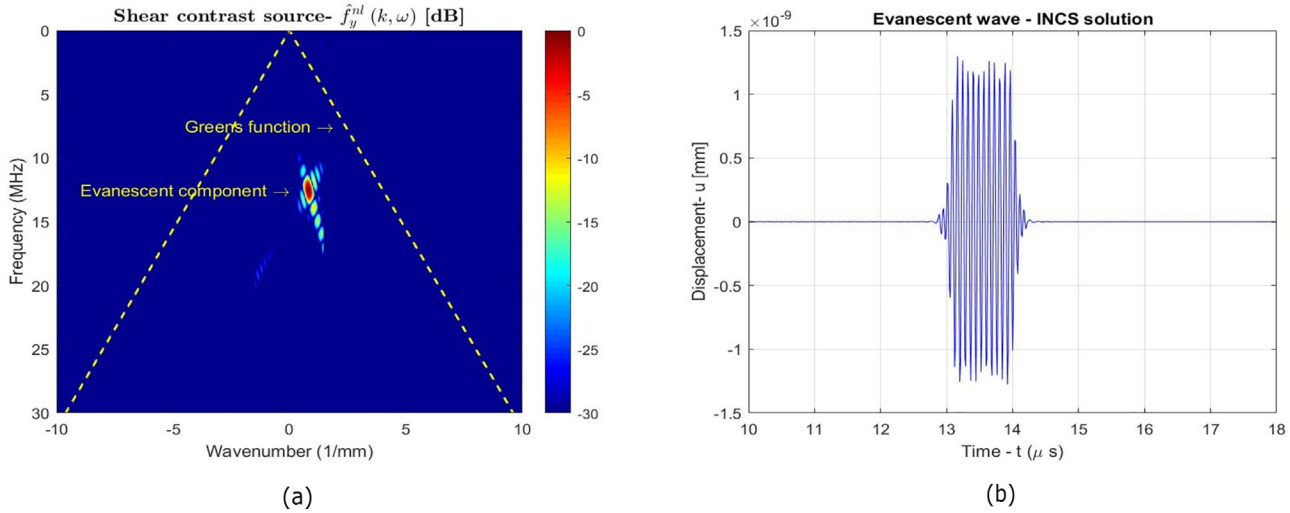

FIG. 9. (Color online) The evanescent wave depicted by the (a) nonlinear shear contrast source, $\hat{f}_y^{nl}(k, \omega)$ and (b) evanescent waveform generated by two-way mixing.

https://doi.org/10.1121/10.0010448

an extension of the presented approach toward a full 3D nonlinear elastic wave problem in the future.

ACKNOWLEDGMENTS

This research work was supported by the Delft University of Technology and TNO, the Netherlands. The authors would like to thank Dr. Jianmin Qu and Dr. Youxuan Zhao for providing the reference solution.

[1]A. N. Norris, "Finite-amplitude waves in solids," in *Nonlinear Acoustics*, edited by M. F. Hamilton and D. T. Blackstock (Acoustical Society of America, Melville, NY), pp. 263–277 (1998).
[2]A. Demčenko, "Development and analysis of noncollinear wave mixing techniques for material properties evaluation using immersion ultrasonics," Ph.D. thesis, University of Twente, Enschede, The Netherlands, 2014.
[3]S. Eldevik, "Measurement of non-linear acoustoelastic effect in steel using acoustic resonance," Ph.D. thesis, University of Bergen, Bergen, Norway, 2014.
[4]L. K. Zarembo and V. A. Krasil'nikov, "Nonlinear phenomena in the propagation of elastic waves in solids," Sov. Phys. Usp. **13**, 778–797 (1971).
[5]K. H. Matlack, J.-Y. Kim, L. J. Jacobs, and J. Qu, "Review of second harmonic generation measurement techniques for material state determination in metals," J. Nondestr. Eval. **34**, 273 (2015).
[6]G. Tang, M. Liu, L. J. Jacobs, and J. Qu, "Detecting localized plastic strain by a scanning collinear wave mixing method," J. Nondestr. Eval. **33**, 196–204 (2014).
[7]M. D. Verweij and J. Huijssen, "A filtered convolution method for the computation of acoustic wave fields in very large spatiotemporal domains," J. Acoust. Soc. Am. **125**, 1868–1878 (2009).
[8]J. Huijssen and M. D. Verweij, "An iterative method for the computation of nonlinear, wide-angle, pulsed acoustic fields of medical diagnostic transducers," J. Acoust. Soc. Am. **127**, 33–44 (2010).
[9]J. Huijssen, "Modeling of nonlinear medical diagnostic ultrasound," Ph.D. thesis, Delft University of Technology, Delft, The Netherlands, 2008, available at http://repository.tudelft.nl (Last viewed April 22, 2022).
[10]L. Demi, "Modeling nonlinear propagation of ultrasound through inhomogeneous biomedical media," Ph.D. thesis, Delft University of Technology, Delft, The Netherlands, 2013.
[11]L. Demi, K. van Dongen, and M. D. Verweij, "A contrast source method for nonlinear acoustic wave fields in media with spatially inhomogeneous attenuation," J. Acoust. Soc. Am. **129**, 1221–1230 (2011).
[12]M. D. Verweij, L. Demi, and K. van Dongen, "Computation of nonlinear ultrasound fields using a linearized contrast source method," J. Acoust. Soc. Am. **134**, 1442–1453 (2013).
[13]G. L. Jones and D. R. Kobett, "Interaction of elastic waves in an isotropic solid," J. Acoust. Soc. Am. **35**, 5–10 (1963).
[14]Z. Chen, G. X. Tang, Y. Zhao, L. J. Jacobs, and J. Qu, "Mixing of collinear plane wave pulses in elastic solids with quadratic nonlinearity," J. Acoust. Soc. Am. **136**(5), 2389–2404 (2014).
[15]M. H. Liu, G. X. Tang, L. J. Jacobs, and J. Qu, "Measuring acoustic nonlinearity parameter using collinear wave mixing," J. Appl. Phys. **112**(2), 024908 (2012).
[16]V. A. Korneev and A. Demčenko, "Possible second-order nonlinear interactions of plane waves in an elastic solid," J. Acoust. Soc. Am. **135**(2), 591–598 (2014).
[17]G. X. Tang, L. J. Jacobs, and J. Qu, "Scattering of time-harmonic elastic waves by an elastic inclusion with quadratic nonlinearity," J. Acoust. Soc. Am. **131**(4), 2570–2578 (2012).
[18]S. Kücher, T. Meurer, L. J. Jacobs, and J. Qu, "Two-dimensional wave propagation in an elastic half-space with quadratic nonlinearity: A numerical study," J. Acoust. Soc. Am. **125**(3), 1293–1301 (2009).
[19]K. R. McCall, "Theoretical study of nonlinear elastic wave propagation," J. Geophys. Res. **99**, 2591–2690, https://doi.org/10.1029/93JB02974 (1994).
[20]A. Demčenko, M. Mazilu, J. Reboud, and J. M. Cooper, "Green-function method for nonlinear interactions of elastic waves," in *2019 IEEE International Ultrasonics Symposium (IUS)* (2019), pp. 1859–1861.
[21]M. Mazilu, A. Demčenko, R. Wilson, J. Reboud, and J. M. Cooper, "Breaking the symmetry of momentum conservation using evanescent acoustic fields," Phys. Rev. Lett. **121**, 244301 (2018).
[22]J. Rushchitsky, *Nonlinear Elastic Waves in Materials* (Springer International, Switzerland, 2014).
[23]D. T. Blackstock, "Generalized Burgers equation for plane waves," J. Acoust. Soc. Am. **77**, 2050–2053 (1985).
[24]Q. Liu, "Generalization of the *k*-space formulation to elastodynamic scattering problems," J. Acoust. Soc. Am. **97**, 1373–1379 (1995).
[25]F. R. Rollins, "Interaction of ultrasonic waves in solid media," Appl. Phys. Lett. **2**(8), 147–148 (1963).
[26]A. Demčenko, R. Akkerman, P. B. Nagy, and R. Loendersloot, "Non-collinear wave mixing for non-linear ultrasonic detection of physical ageing in pvc," NDT&E Int. **49**, 34–39 (2012).
[27]M. Morlock, J. Kim, L. J. Jacobs, and J. Qu, "Mixing of two co-directional Rayleigh surface waves in a nonlinear elastic material," J. Acoust. Soc. Am. **137**(1), 281–292 (2015).